Subscriber access provided by READING UNIV

Article

In vivo evaluation of folate decorated crosslinked micelles for the delivery of platinum anticancer drugs

Martina Heide Stenzel

Biomacromolecules, **Just Accepted Manuscript** • DOI: 10.1021/bm501558d • Publication Date (Web): 28 Dec 2014

Downloaded from http://pubs.acs.org on January 4, 2015

Just Accepted

"Just Accepted" manuscripts have been peer-reviewed and accepted for publication. They are posted online prior to technical editing, formatting for publication and author proofing. The American Chemical Society provides "Just Accepted" as a free service to the research community to expedite the dissemination of scientific material as soon as possible after acceptance. "Just Accepted" manuscripts appear in full in PDF format accompanied by an HTML abstract. "Just Accepted" manuscripts have been fully peer reviewed, but should not be considered the official version of record. They are accessible to all readers and citable by the Digital Object Identifier (DOI®). "Just Accepted" is an optional service offered to authors. Therefore, the "Just Accepted" Web site may not include all articles that will be published in the journal. After a manuscript is technically edited and formatted, it will be removed from the "Just Accepted" Web site and published as an ASAP article. Note that technical editing may introduce minor changes to the manuscript text and/or graphics which could affect content, and all legal disclaimers and ethical guidelines that apply to the journal pertain. ACS cannot be held responsible for errors or consequences arising from the use of information contained in these "Just Accepted" manuscripts.

ACS Publications
High quality. High impact.

Biomacromolecules is published by the American Chemical Society. 1155 Sixteenth Street N.W., Washington, DC 20036

Published by American Chemical Society. Copyright © American Chemical Society. However, no copyright claim is made to original U.S. Government works, or works produced by employees of any Commonwealth realm Crown government in the course of their duties.

This document is confidential and is proprietary to the American Chemical Society and its authors. Do not copy or disclose without written permission. If you have received this item in error, notify the sender and delete all copies.

In vivo evaluation of folate decorated crosslinked micelles for the delivery of platinum anticancer drugs

Journal:	*Biomacromolecules*
Manuscript ID:	bm-2014-01558d.R1
Manuscript Type:	Article
Date Submitted by the Author:	18-Dec-2014
Complete List of Authors:	Eliezar, Jeaniffer; University of New South Wales, Scarano, Wei; University of New South Wales, Boase, Nathan; The University of Queensland, Australian Institute for Bioengineering and Nanotechnology and Centre for Advanced Imaging Thurecht, Kristofer; The University of Queensland, Australian Institute for Bioengineering and Nanotechnology and Centre for Advanced Imaging Stenzel, Martina; University of New South Wales,

SCHOLARONE™
Manuscripts

In vivo evaluation of folate decorated crosslinked micelles for the delivery of platinum anticancer drugs

Jeaniffer Eliezar[a], *Wei Scarano*[a], *Nathan R. B. Boase*[b], *Kristofer J. Thurecht*[b*] *Martina H. Stenzel*[a*]

[a]Centre for Advanced Macromolecular Design (CAMD), School of Chemistry, University of New South Wales, Sydney, NSW 2052, Australia

[b]Centre for Advanced Imaging (CAI) and Australian Institute for Bioengineering and Nanotechnology, ARC Centre of Excellence in Convergent Bio-Nano Science and Technology, The University of Queensland, St Lucia, QLD 4072, Australia

Email: K.Thurecht@uq.edu.au, M.Stenzel@unsw.edu.au

Abstract

The biodistribution of micelles with and without folic acid targeting ligands were studied using a block copolymer consisting of acrylic acid (AA) and polyethylene glycol methyl ether acrylate (PEGMEA) blocks. The polymers were prepared using RAFT polymerization in the presence of a folic acid functionalized RAFT agent. Oxoplatin was conjugated onto the acrylic acid block to form amphiphilic polymers which, when diluted in water, formed stable micelles. In order to probe the in vivo stability, a selection of micelles were crosslinked using 1,8-diamino octane. The sizes of the micelles used in this study range between 64-200 nm, with both spherical and worm-like conformation.

The effects of crosslinking, folate conjugation and different conformation on the biodistribution were studied in female nude mice (BALB/c) following intravenous injection into the tail vein. Using optical imaging to monitor the fluorophore-labelled polymer, the *in vivo* biodistribution of the micelles was monitored over a 48 hour time-course after which the organs were removed and evaluated *ex vivo*.

These experiments showed that both crosslinking and conjugation with folic acid led to increased fluorescence intensities in the organs, especially in the liver and kidneys, while micelles that are not conjugated with folate and/or not crosslinked are cleared rapidly from the body. Higher accumulation in the spleen, liver and kidneys was also observed for micelles with worm like shapes compared to the spherical micelles.

While the various factors of crosslinking, micelle shape and conjugation with folic acid all contribute separately to prolong the circulation time of the micelle, optimization of these parameters for drug delivery devices could potentially overcome adverse effects such as liver and kidney toxicity.

Introduction

Polymeric micelles are self-assembled macromolecular structures constituting amphiphilic block copolymers. These micelles stand out from various types of drug carriers due to their core-shell structure and easily tunable size and surface properties.[1] The nature of the constituent block copolymers influences the properties of the micelle such as size, which is ideally between 20-100 nm for drug delivery applications. Thus, with proper formulation, nanoparticles could be synthesized above the size range required to surpass the typical renal filtration cutoff (5 nm) to prevent rapid clearance. [2-4] Their relatively small size also gives them the advantage of reduced recognition by the phagocytic cells of the reticuloendothelial system (RES), which can assist in prolonged blood circulation. [5] In addition, their passive accumulation in solid tumors through the enhanced permeability and retention (EPR) mechanism[6, 7] makes these core-shell particles a valid choice for a drug delivery system.

Polymeric micelles have been frequently investigated *in vivo* as drug delivery vehicles. However, the dynamic nature of micelles may lead to disassembly *in vivo* which ultimately affects their cellular uptake [8, 9] and also biodistribution. This is overcome in many ways through crosslinking [10] which locks in the spherical conformation of the micelle. This can in turn increase circulation time compared to the uncrosslinked counterparts, which subsequently leads to increased accumulation in the tumor environment. [11-13] Direct comparison between crosslinked and uncrosslinked micelles revealed a much higher accumulation of the crosslinked micelles in the tumor, while the buildup in liver and kidney were similar for both systems. [11] However, the fate of these nanoparticles is not always clear in an *in vivo* environment; crosslinked micelles generally have a lower accumulation in the liver than their uncrosslinked counterparts,[12] yet it may encourage the build-up in other organs such as the spleen.[12] Ultimately, these initial findings suggest that the final destination of these particles is determined by an array of parameters, but is predominantly dictated by their surface chemistry. Complete understanding of these effects in animals has yet to be achieved, as only preliminary studies have been undertaken to explore this phenomenon. Indeed, these reported *in vivo* experiments in mice have led to more questions surrounding the stability and biodistribution of the nanoparticles.

The importance of surface PEGylation of crosslinked micelles has been highlighted in earlier reports where the increased fraction of PEG chains directly reduced accumulation in the liver

and spleen while enhancing circulation time.[14] The accumulation of crosslinked micelles can be further reduced by adjusting the amount of PEG on the surface by using mixed micelles, which were based on two different block copolymers.[15] Interestingly, the fully PEGylated crosslinked micelles did not display the longest circulation time or the lowest accumulation in liver and spleen. It was argued that introduction of a certain amount of hydrophobic groups into the micelle surface may make the nanoparticle resemble protein structures, which can help evade clearance by the liver and the kidney.[15] Most crosslinked micelles investigated were typically between 50 and 100 nm in size, but also smaller micelles such as those obtained from the self-assembly of redox-responsive telodendrimers were shown to enhance the circulation time and improve tumor uptake. [13]

It is widely proposed that nanoparticles that exhibit passive accumulation in tumors via the EPR effect can also be modified to adopt an active targeting approach. Decorating the surface of micelles with bioactive functional groups is commonly applied in nanomedicine due to the fact that receptors on cell membranes will selectively interact with ligands that are immobilized on the micelle surface. A popular choice to target cancer cells is via folate receptors, where selected cancer cells over-express folate-binding proteins (FBP) on their surface. [16] There are many reports in literature on the surface functionalization of nanoparticles including micelles [17-21] and when decorated with folate these particles are known to increase the accumulation in tumors which subsequently increases the amount of drug delivered.[22, 23]

The use of folate-decorated surfaces has been used extensively in nanomedicine for targeting tumours, but there are many factors that have not been fully understood. For example, it was demonstrated that the accumulation of doxorubicin in tumors was enhanced when using folate-conjugated micelles as delivery vehicles and this also coincided with longer circulation and higher blood concentrations.[24] However, the amount of folate-labelled particles in the tumor is not always higher compared to naked PEGylated particles. This highlights the complexity of the mechanisms involved in active targeting nanoparticles for drug delivery applications [25-28]. It was argued that this particular effect might be due to non-specific protein absorption that takes place upon injection into serum and this masks the targeting agent and prevents interaction with the desired receptor on cell surfaces.[29]

The biodistribution of nanoparticles is influenced by both the surface functionality and its stability. Comparing micelles with and without folate-targeting revealed a higher accumulation of drug in the tumor when delivered using folate decorated micelles. Previous studies have shown that both types of micelles reduced the accumulation of doxorubicin in most organs except liver.[30] Finally, a comparison of crosslinked micelles with and without folate targeting demonstrated that the crosslinked version showed higher accumulation in liver; however, in this particular case neither version enhanced particle accumulation in tumor.

Despite the advantages and the prevalence of folate-conjugated micelles as an active target delivery system, the effect of folate ligand and crosslinking on particle biodistribution have not yet been thoroughly studied. Here we report directly on the biodistribution of crosslinked and non-crosslinked micelles in mice, and then assesses the effectiveness of folate-decorated micelles in targeting tumors. In addition, the effect of the particle shape was also evaluated. Block copolymers were prepared as outlined in Scheme 1. The hydrophilic polymer was synthesized using polyethylene glycol methyl ether acrylate as the shell, while the core forming block consisted of acrylic acid. Owing to the importance of platinum drugs in the treatment of cancer,[31-34] oxoplatin was then conjugated to the acrylic acid block, leading to an amphiphilic copolymer that subsequently self-assembled in aqueous solution to form micelles. The micelle was then crosslinked using established procedures to further stabilize the micelle.

Molecular imaging has emerged as a non-invasive approach for evaluating effectiveness of drug delivery systems. Compared to other diagnostic methods such as biopsies, molecular imaging provides minimum disruption to the subject, and allows for the same subject to be monitored at multiple time points over the course of a treatment. [35] Modern molecular imaging techniques, utilizing polymeric molecular imaging agents have made it possible to study particle biodistribution *in vivo* with high sensitivity and yielding high resolution images. In this study, the biodistribution of nanoparticles will be monitored via fluorescence imaging and X-Ray imaging. The polymers used in the study are labelled with an organic fluorophore either before or after micelles were formed.

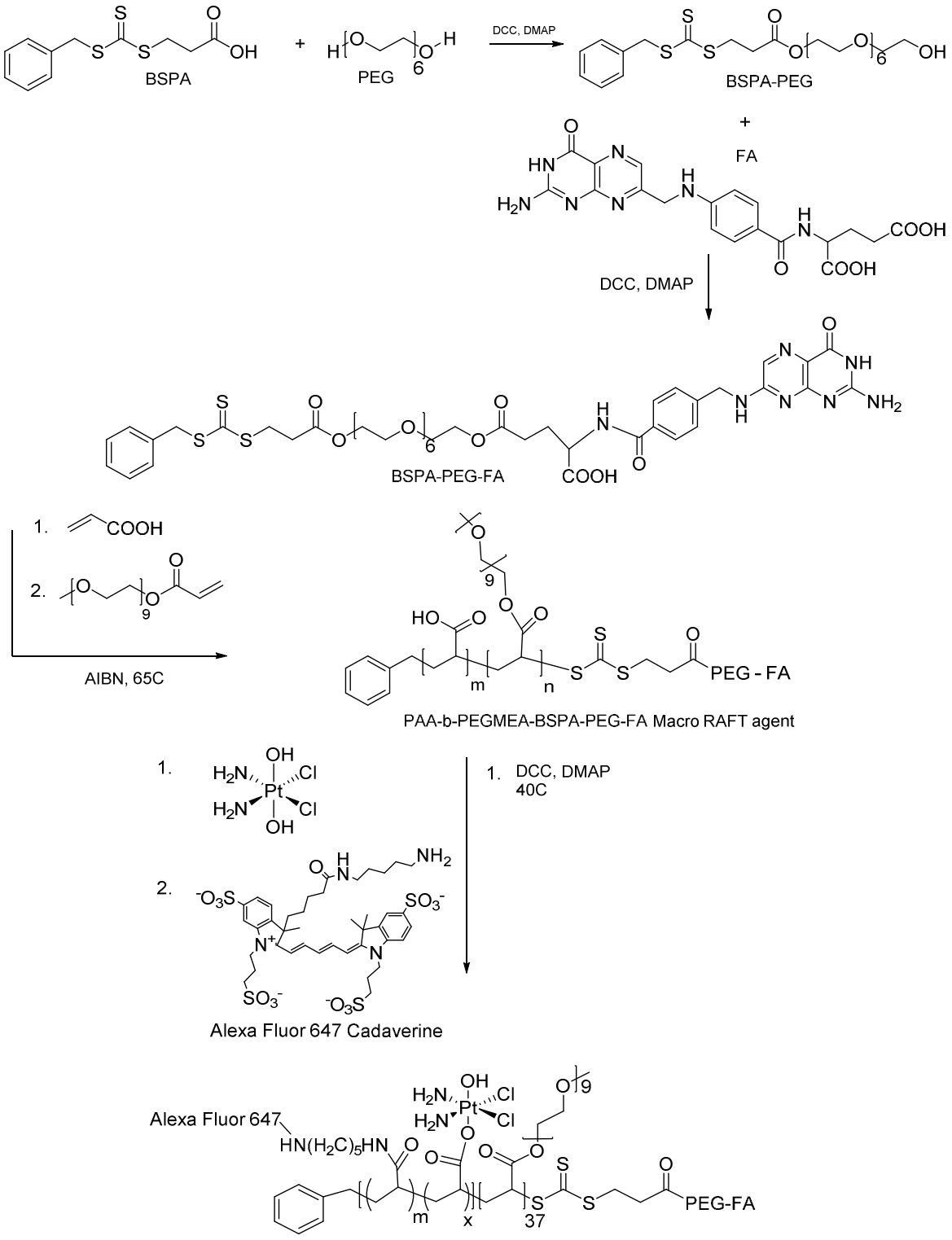

Scheme 1. Synthesis of BSPA-PEGMEA-PEG-FA and the conjugation of dye and drug

Experimental section

Materials

Folic Acid (Aldrich, >97%), 2,2-Azobisisobutyronitrile (AIBN; Fluka, 98%), : Poly(ethylene glycol) (PEG; M_n= 300 g mol^{-1}, Sigma Aldrich), *N,N'*-dicyclohexylcarbodiimide (DCC; Aldrich, 99%), *cis*-diammineplatinum (II) dichloride (CDDP; Aldrich, 99.9%), *N*-(3-Dimethylaminopropyl)-*N*′-ethylcarbodiimide hydrochloride (EDC; Aldrich, 98%), *N,N'*-dicyclohexylcarbodiimide (DCC; Aldrich, 99%), *N*-hydroxysuccinimide (NHS; Aldrich, 98%), 3-(benzylsulfanylthiocarbonylsuIfanyl) propionic acid (BSPA) RAFT agent, 4-(dimethylamino) pyridine (DMAP; Aldrich, 99%) and 2,2-Azobisisobutyronitrile initiator (AIBN; Fluka, 98%), *N,N*-dimethylformamide (DMF; Aldrich), 1,8-diamino octane (Aldrich, >99%), hydrogen peroxide (H_2O_2; Ajax Fine Chem, 30 % w/v), isoflurane solution (BOMAC), 10x Phosphate buffered saline (PBS; Biowhittaker).

Acrylic acid (AA, M_n= 72.06 g mol^{-1}, Aldrich, 99%) and Polyethylene glycol methyl ether acrylate (PEGMEA, M_n= 480 g mol^{-1}, Aldrich) were destabilized by passing them over a column of basic alumina and stored at -7^{o}C. Deionized (DI) water was produced by Milli-Q water purification system and has a resistivity of 17.9 mΩ/cm.

Synthesis

Synthesis of RAFT agent

Synthesis of BSPA

BSPA was synthesized according to literature.[36] In short, 3-Mercaptopropanoic acid (5 mL) was added to a solution of potassium hydroxide (6.571 g) in water (62.5 mL). Carbon disulfide (7.5 mL) was added drop wise. The resulting orange solution was stirred for 5 hours. The mixture was then heated with benzyl bromide (10mL, drop wise) at 80^{o}C for 12 hours. The mixture was left to cool to room temperature. Chloroform (75 mL) was added and the mixture was transferred to a separating funnel. Hydrochloric acid (1 M, excess) was added to acidify the mixture until the organic layer turned yellow. The water phase was extracted with 2x50mL Chloroform. The combined organic layers were dried over magnesium sulfate. Purification was done in a column with 3:1 hexane to ethyl acetate solvent mixture. (Yield: 14 g)

Modification of BSPA RAFT agent with PEG

BSPA RAFT agent (0.6427 g, 0.384 mmol), Poly(ethylene glycol) (PEG) (0.6083 g, 0.4224 mmol), DCC (0.4915 g, 0.384 mmol) and DMAP (0.0288 g, 0.0384 mmol) was dissolved in minimum amount of ethyl acetate and stirred overnight in the dark. The product was filtered through cotton wool to remove the white precipitates (urea). The resulting clear yellow solution (crude) was dried and purified by column chromatography.Two steps of gel chromatography was performed to collect the purified product. Firstly, a mixture of 1:5 ethyl acetate/ N-hexane was used to remove the unreacted BSPA. And finally, the PEG conjugated RAFT was obtained with 100% ethanol as a mobile phase of the column to yield a yellow gel..

Synthesis of BSPA-PEG-FA RAFT agent

Folic acid (0.6947 g, 0.157 mmol) was dissolved in minimum amount of DMSO solvent and was stirred overnight. The third fraction of BSPA-PEG RAFT agent prepared previously (0.4 g, 0.787 mmol) was dissolved in minimum amount of DMSO and added into Folic acid solution. DCC (0.1643 g, 0.787 mmol) and DMAP (0.0097 g, 0.0787 mmol) were added into the mixture andstirred overnight in the dark. The resulting mixture was filtered through cotton wool resulting in clear dark orange solution. The solution was dried under reduced vacuum (5mbar, 50 ^{o}C) for 17 hours. The product was purified through precipitation with water (deionised). Cloudy yellow solution and orange precipitates was observed. The solution was freeze dried and analysed by ^{1}H NMR in DMSO.

Synthesis of block copolymers

Acrylic acid and PEGMEA are the constituents for the block copolymer. Three block copolymer samples were prepared, one control (Polymer A) and two folate conjugated block copolymers with different chain length (Polymer B and C). . The absolute quantities used for samples A, B and C can be found in the ESI, Table S1.

Pure BSPA RAFT agent was used without any modification to polymerise the control polymer. PEGMEA was polymerised as the first block, followed by the polymerisation of AA. PEGMEA (1 g, 2.083 mmol), AIBN (0.7 mg, 4.167 μmol), BSPA (11 mg, 0.0416 mmol) were dissolved in Toluene (1.5 mL). The mixture was purged under nitrogen for 30 minutes and polymerised at 65 ^{o}C for 3 hours. The samples were characterised by ^{1}H NMR (ESI, Figure S3 to S8), then purified by dialysis against water (MWCO 3500). After lyophilisation,

the polymer is chain extended with Acrylic acid. AA (34 mg, 0.4162 mmol), AIBN (0.14 mg, 0.8324 mmol), BSPA-PEGMEA (0.1508 g, 8.324 μmol) were dissolved in DMSO (416.2 μL). The mixture were purged under nitrogen and polymerized at 65 ^{o}C for 22 hours. The product was purified by dialysis against water and dried. Summary of the amount of polymerisation reagents and the respective number of moles can be found in ESI, Table S1. In addition, the details of the polymerization conditions can be found in ESI Table S2.

Synthesis of Oxoplatin

Oxoplatin was synthesized according to literature. [37] A mixture of cisplatin (1.0 g, 3.05 mmol) and H_2O_2 30 w/v (3.5 mL, 30.5 mmol) was heated at 70 °C for 5 h. The heat was then removed and the reaction mixture was stirred overnight. The product was recrystallized in situ at 4 °C overnight. The product was obtained by vacuum filtration and washed with ice cold water, ethanol, and diethyl ether. After filtration, the solvent was removed under reduced pressure to give the expected product as bright yellow powder (Yield 90%).

Oxoplatin conjugation

Sample A

Polymer A (20.8 mg, 0.934 μmol), Oxoplatin (2 mg, 4.391 μmol), EDC (1 mg, 4.391 μmol), NHS (0.2 mg, 1.756 μmol and DMAP (0.1 mg, 0.439 μmol)) were mixed in DMF (1 mL) and stirred (48 h) in the dark. The product was then centrifuged for 5 minutes at 7,000 rpm to obtain a clear yellow solution and a pale yellow precipitate. The clear yellow supernatant is the oxoplatin conjugated polymer. The solution was filtered to remove any unreacted oxoplatin through a 0.45μm filter.

Sample B

Polymer B (20.5 mg, 0.915 μmol) was combined with Oxoplatin (1.8 mg, 4.853 μmol), EDC (1 mg, 4.853 μmol), NHS (0.5 mg, 1.94μmol) and DMAP (0.1 mg, 0.485 μmol)were dissolved in DMF (1 mL) and stirred (48 h) in the dark. The product was centrifuged for 5 minutes at 7,000rpm and the supernatant was filtered through 0.45 μm filter.

Sample C

Polymer C (42.9 mg, 2.520 μmol), Oxoplatin (15 mg, 0.18 mmol), EDC (5.3 mg, 0.018 mmol) NHS (0.6 mg, 5.52μmol) and DMAP (0.2 mg, 1.840 μmol) was combined. The mixture was dissolved in DMF (1 mL) and stirred (48 h) in the dark. The product was

centrifuged (5 minutes, 7,000 rpm) and the clear yellow supernatant was filtered through 0.45 μm syringe filter.

The polymer was transferred into a vial to be labelled with dye and subsequently formulated into micelles. The polymer was labelled with fluorophore, followed by micelle formation.

Dye conjugation

Alexa Fluor 647 Cadaverine, disodium salt was chosen as the dye for the study. The polymers were labelled with NHS coupling agent during the oxoplatin conjugation reaction as a conjugation site of the dye. A stock solution of 1 mg/mL was made by diluting 1 mg of the dye in 1 mL DMF solvent. 100 μL of the stock solution were added to 2 mL of sample A, B, and C (dye concentration is 0.048 mg/mL).The blue solution was stirred overnight in the dark and then purified by dialysis against MilliQ water (MWCO 3500).

Micelle formation and crosslinking

Micelles were formed by adding water with 1:1 water to DMF ratio. 1 mL of water was added to each of the sample with the rate of 0.1 mL/hour with continuous stirring. The products were dialyzed against water under dark.

1,8-diamino octane (3 mg; 2.05 x 10^{-2} mmol) and EDC (2 mg; 1.29 x 1^{-2} mmol) were added to the solution of dialyzed micelles of sample A, B and C (20 mg polymer in 2 mL solution) for crosslinking. The reaction mixture was left to stir for 24 h and followed by dialysis against DI water for overnight with frequent water change using membrane (MWCO 3500).

Analysis

Inductively Coupled Plasma-Mass Spectrometer (ICP-MS)

An Inductively Coupled Plasma-Mass Spectrometer (ICP-MS) was employed to quantify the amount of oxoplatin attached to the polymer (The Perkin-Elmer ELAN 6000). All experiments were carried out at an incident ratio frequency power of 1200 W. The plasma argon gas flow of 12 L min^{-1} with an auxiliary argon flow of 0.8 L min^{-1} was used in all cases. The nebulizer gas flow was adjusted to maximize ion intensity at 0.93 L min^{-1} as indicated by the mass flow controller. The element/mass detected was ^{195}Pt and the internal standard used was ^{193}Ir. Replicate time was set to 900 ms and the dwell time to 300 ms. Peak hopping was the scanning mode employed and the number of sweeps/readings was set to 3.

Ten replicates were measured at a normal resolution. The samples were treated with aqua regia solution at 90 °C for 2 h to digest platinum.

The samples were prepared using acid digestion by mixing 100 μL of polymer with aqua regia (9.90 mL). The solution was then heated up to 90^{o}C overnight. The heat was removed and the sample was analyzed.

Transmission electron microscopy (TEM)

The TEM micrographs were obtained using a JEOL 1400 transmission electron microscope operating at an accelerating voltage of 100 kV. The samples were prepared by casting the micellar solution (1 mg mL-1) onto a formvar-coated copper grid, followed by slow evaporation of the aqueous phase. No staining was applied.

In vivo biodistribution

All animal experiments were undertaken according to University of QLD ethics (AIBN/400/13/ARC/NHMRC). Female BALB/c nude mice were purchased from Animal Resource Centre in Perth WA.

The injection samples were prepared by diluting 225 μL of the polymeric micelles with 25μL of concentrated PBS which gave a final polymer concentration of (9 mg/mL). 100 μL of the drug solution was injected intravenously into the tail vein. Longitudinal imaging studies were performed, where the mice were imaged at multiple time points over a 48 hour period (0, 1, 6, 24 and 48hr after injection). Mice were imaged under fluorescence and X-ray at every time point using a Bruker MS-FX Pro optical scanner. The mice were culled after the final imaging time point (48 h) and tissues of interest were harvested and imaged *ex vivo*.

Three parameters were investigated as part of this study: 1) the behavior of folate-labelled nanoparticles; 2) the effect of crosslinking; and 3) the effect of morphology on the biodistribution of the nanoparticles *in vivo* (Scheme 2). Each set of experiments were undertaken in duplicate to cover statistical variation of the results.

Phantom solutions of the micelles were imaged prior to injection to obtain relative fluorescence intensities of each polymer subset. This control experiment confirmed that the samples had similar intensities allowing direct comparison of all samples between sets. (ESI, Figure S18)

In vivo fluorescence Imaging

In vivo optical imaging experiments were performed on an In Vivo MS FX Pro instrument (now supplied by Bruker Corporation). Alexa Fluor-647 images were collected with a 630 ± 10 nm excitation and 700 nm ± 17.5 nm emission filter set (f- stop 2.80, 4 × 4 binning, 120 mm FOV, 60 sec exposure time). To provide anatomical context, fluorescence images were co-registered with an X-ray image (f-stop 2.80, 0.2 mm aluminum filter, 120 mm FOV, 30 sec acquisition time). All images were batch exported as 16-bit TIFF images and image processing was completed using Image-J (National Institutes of Health). Fluorescence images were false colored and overlaid onto X-ray images.

Results and discussions

Synthesis and physical characterization of polymers and micelles

In order to reproducibly label the polymers with folic acid (FA), a novel RAFT agent was synthesized that incorporated the FA onto the Z-group of polymer. This ensured that each chain was terminated with the targeting ligand, FA. To achieve this end, the RAFT agent BSPA was PEGylated with PEG300 (PEG molecular weight 300 g mol^{-1}) prior to attachment of FA as depicted in Scheme 1. The conjugation of PEG introduced a more flexible and less sterically-hindered linker for the subsequent reaction with folic acid compared to unmodified BSPA. The success of the reaction was confirmed by ^{1}H NMR (ESI, Figure S1). A test of solubility showed that the PEG-modified RAFT agent was soluble in both water and diethyl ether, while the unmodified BSPA was only soluble in the organic solvent.

FA was attached via DCC-DMAP coupling to the terminal hydroxyl group of the BSPA-PEG. Owing to the poor solubility of FA in water, it was first dissolved in DMSO prior to the reaction. The viscous folic acid solution tended to form a gel, thus prolonged mixing was necessary to ensure complete dissolution. After isolation of the product, the structure of the desired compound was confirmed using ^{1}H NMR (ESI, Figure S2). It should be noted that this reaction usually leads to a mixture of two products, where the ester to the folic acid is either generated with the carboxygroup in α-position or the γ-position (as shown in Scheme 1). It is important to note that 65% of the FA-NHS conjugate is γ-isomer, while the a-isomer is considered biologically inactive.[38] Unfortunately separation of α and γ isomers is deemed difficult.

Both BSPA-PEG-FA and unmodified BSPA were employed in the synthesis of block copolymers. PEGMEA and AA were polymerized as the first and second block of the copolymer, respectively. The chain length of PEGMEA block was kept constant at 20-30 units, while the block size of the AA was varied to generate micelles of different sizes. Due to the position of the folic acid on the Z-group of the macro RAFT agent, AA had to be polymerized as the first block to ensure that folic acid was located at the surface of the micelle. The conversion of the polymerization was determined using ^{1}H-NMR as shown in ESI, FigS3-S8. It should be noted that the polymers have a significant tendency to interact with the column material and therefore the measured molecular weight values were found to be higher than the theoretical values.

The final polymers containing blocks of PEGMEA and AA were initially fully soluble under aqueous conditions. The amphiphilic block copolymers used in the study were subsequently formed through the conjugation of acid groups with oxoplatin, which renders the polyacrylic acid block hydrophobic.[38] The success of oxoplatin conjugation to the polymer can thus be qualitatively confirmed by measuring the amphiphilic nature of the block copolymer where the polymer self-assembles into micelles in aqueous solution.

Oxoplatin has only limited solubility in many common solvents. Out of a large range of common solvents, DMF was found to exhibit the highest solvation of the drug, albeit only partial solubility. The conjugation reaction was then carried out using a 1:1 molar ratio of the drug oxoplatin to the acrylic acid repeating units. In addition, vigorous and prolonged mixing was also applied to mitigate the solubility issue of the drug as well as ensuring a high efficiency of drug conjugation.

The amount of platinum drug coordinated to the polymer was measured using ICP-MS and the results are tabulated in Table 1. Interestingly, lower conjugation was observed for the folate-labelled samples compared to the control samples. It is likely that the low solubility of folic acid lead to poor presentation of the acrylic acid groups in the final polymer, therefore limiting the access of oxoplatin to the reactive acid groups. Moreover, the low solubility of oxoplatin in the solution also lowers the diffusion of the drug molecule, which in turns decreases the efficiency of conjugation.

In order to monitor the fate of the nanoparticles in an *in vivo* environment, the micelles were labelled by NIR-dye Alexa Fluor 647 Cadaverine disodium salt to facilitate tracking using optical imaging. The sequence of the dye and drug conjugation was varied in order to study the influence of incorporating the various species on the micelle size or shape. Samples A and B were fluorescently-labelled after oxoplatin conjugation, while sample C was labelled before the incorporation of the drug. It was observed that the order of reaction had an interesting effect on the shape of the resulting aggregates. Sample C appeared to possess worm-like morphology, which suggests the formation of higher order assemblies when larger hydrophobic:hydrophilic ratios were employed.

The sizes of micelles A and B were found to be mainly dependent on the drug loading, while the influence arising from variation in the size of the polymer itself were negligible. We hypothesize that high drug loading efficiency led to higher hydrophobicity, and hence the

formation of larger aggregates. The sizes of micelles after the dye conjugation were determined by TEM (Table 1; Table 3, ESI, Figure S9-S14) and DLS (ESI, Fig. S15-S17).

Three different polymers were used for the preparation of micelles and a full list of physical properties is presented in Table 1. In order to increase the structural stability of the micelles, diamine linker was used to crosslink a subset of the particles. This provided a series of nanoparticles having a variety of structural properties for investigation. The different nanoparticles used in this study are illustrated in scheme 2, and include the standard micelle (A), a crosslinked micelle (AX) and two folate-labelled and crosslinked micelles (BX and CX). This provided a means to investigate the effect of size, stability, surface targeting and morphology on biodistribution in animals.

Table 1. Platinum conjugation percentage, size distribution and chain length data for all samples. (X indicates crosslinked samples)

	Sample Name	Polymer	Pt content (w/w%)	ζ potential (mV)	Size (nm)	
					Before crosslinking (TEM)/nm	After crosslinking (X) (TEM)/nm
No Folate	A or AX	PAA_{47}-$PEGMEA_{32}$	3.7%	-17.23	115	95
Folate	BX	PAA_{51}-$PEGMEA_{33}$	0.76%	-14.9	60	75
	CX	PAA_{73}-$PEGMEA_{20}$	0.4%	-17.36	120 (non-spherical)	200 (non-spherical)[a)]

a) Aspect ratio approximately 3 as determined using TEM

Table 2. Representative TEM pictures of the micelles employed in this study. The samples used in this study are highlighted in bold

	Sample Name	TEM Images	
		Crosslinked	Uncrosslinked
Control	Sample **A (right)** **AX (left)**	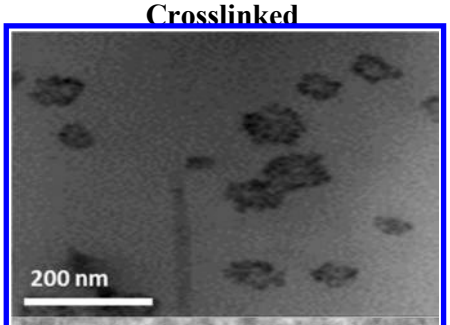	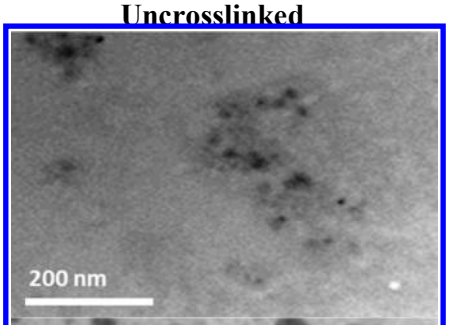
Folate conjugated	Sample B (right) **BX (left)**	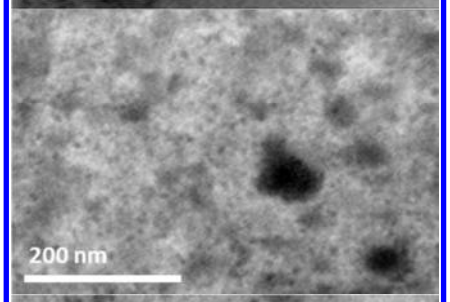	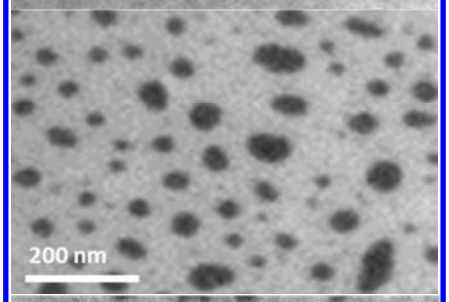
	Sample C (right) **CX (left)**	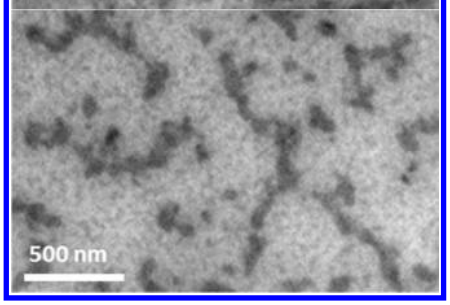	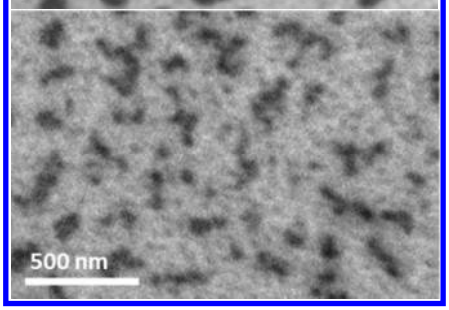

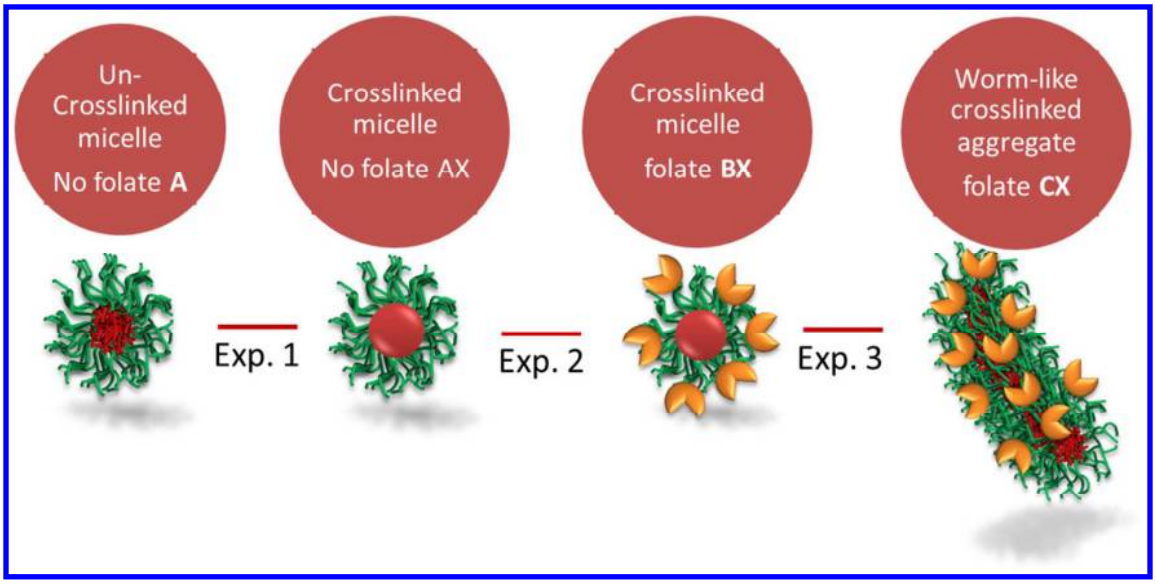

Scheme 2. Nanoparticles employed for the investigation of the biodistribution

The effect of crosslinking (Exp. 1, Figure 2)

The effect of crosslinking was explored using the control polymer with no targeting ligand attached (Scheme 2).

Following intravenous injection of micelles into the tail vein of a mouse, fluorescence images of the non-targeted control polymer (non-folate labelled) samples (A and AX) were compared in Figure 2. Images of the belly and the back side of the mice were taken to display the kidney and liver signals at the respective areas in the body. These images showed that crosslinked micelles have longer circulation time in the animal compared to the uncrosslinked analogue, indicated by higher signal in the kidney in mouse AX compared to no kidney signal in mice A (Figure 2 I). The block copolymers in the uncrosslinked form (most likely existing as unimers from dissociated micelles) experience direct clearance by renal excretion. This is indicated by the fluorescence signal detected in the bladder region 1 hour following injection (Sample A in Figure 2 I). In the crosslinked micelle experiment, an increase in kidney signal can be seen up to six hours, which is showing continual excretion. There is then a decrease in this signal at 24 hours, which remains constant to 48 hours. This suggests that there is a certain portion of the polymers which are above the renal threshold and are not able to be cleared by the kidneys (sample AX in Figure 2I). This phenomenon is not observed in the uncrosslinked polymer This is in agreement with other *in vivo* and *in vitro* experiments from literature,[10-13] where it has been reported that crosslinking enhances the stability of the micelle. In contrast, uncrosslinked micelles would dissociate due to dilution (below CMC value, or through change in structure arising from interactions with biological media) in addition to the effect of other physiological conditions (e.g. increased pressure within the blood vessels).

Ex vivo analysis of both mice was used to validate the information obtained from the *in vivo* images. The mouse treated with the non-crosslinked naked micelle, showed low fluorescence signal across all organs (Figure 2 II, right). This supports the findings from *in vivo* imaging. The signal in the liver of mouse A is hypothesized to be due to dissociation of the polymer chains which exposes the acrylic acid blocks. The acid groups could be interacting with proteins in the blood, which can then be recognized by the RES system. This would then lead to excretion through the gut, which can also be seen in Figure 2II.This result, together with the signals in the bladder region of mouse A at 1 hour (Figure 2 I, top) confirm that

uncrosslinked micelles almost immediately dissociate and are cleared through multiple pathways from the body.

In contrast, the fluorescence signal arising from sample AX – crosslinked micelle – remains constant in the kidneys up to 48 hours (Figure 2 I, bottom) with minimal liver signal observed. This implies that the micelles are unable to be excreted via the renal system. This shows that crosslinking the particle has provided structural integrity to the micelles, allowing them to stay intact in the body and thus resulted in higher circulation concentration in the animal (Figure 2 III). This result is supported by the *ex vivo* images, which shows only significant fluorescence intensity from the kidneys. There is lower signal in the liver, compared to the uncrosslinked micelle, which is due to the protective layer of PEGMEA shielding the charged groups and minimizing clearance via RES.

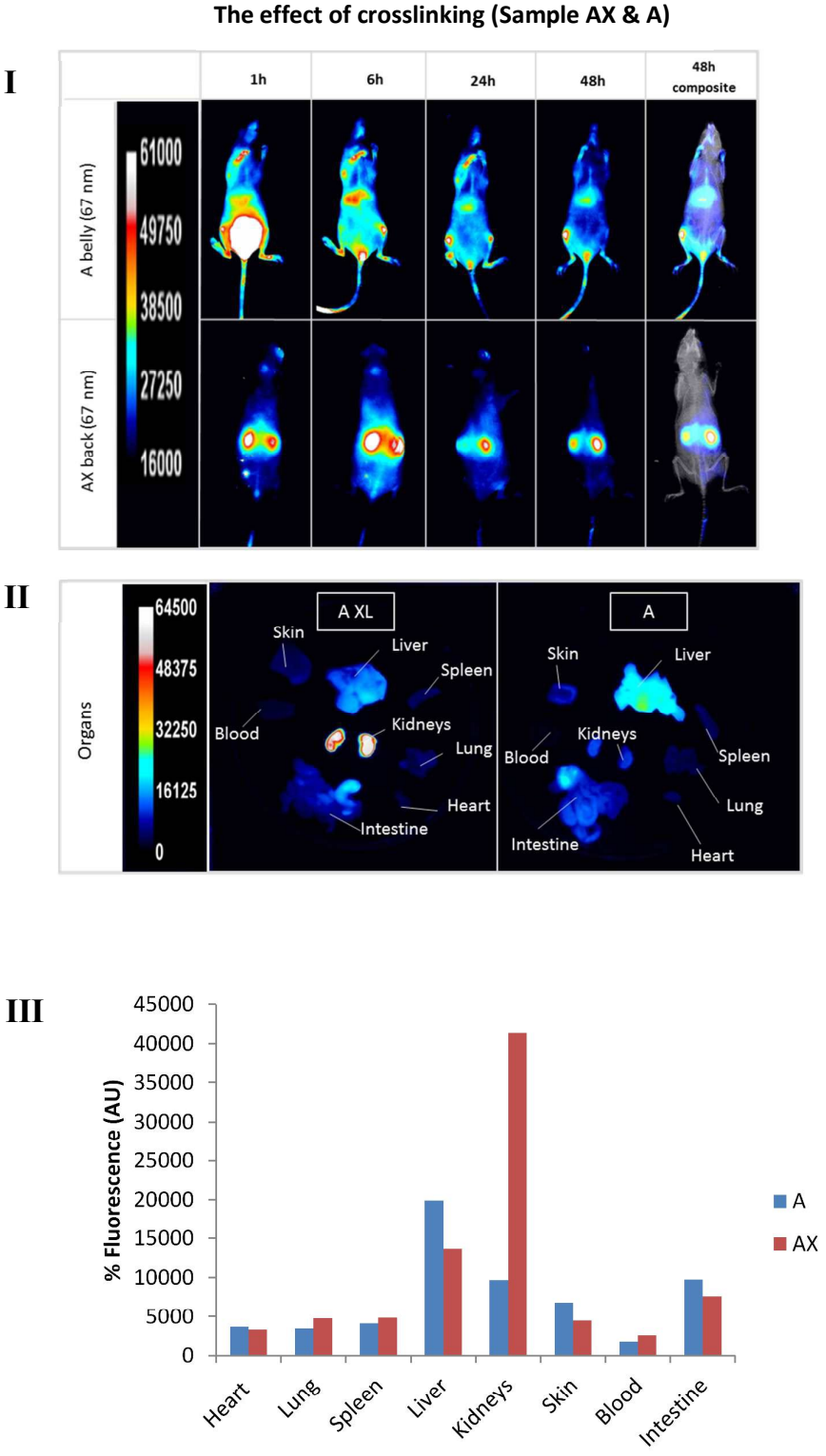

Figure 2. Experiment 2: Crosslinking effect with control samples. (I) In vivo fluorescence mice image (front and back side) of Sample A (uncrosslinked) and AX at 0, 1, 6, 24 and 48hr time courses. (II) Organ fluorescence reflectance image at 48 hr of sample A and AX. (III) Intensity comparison of A and AX in the organs after 48hr.

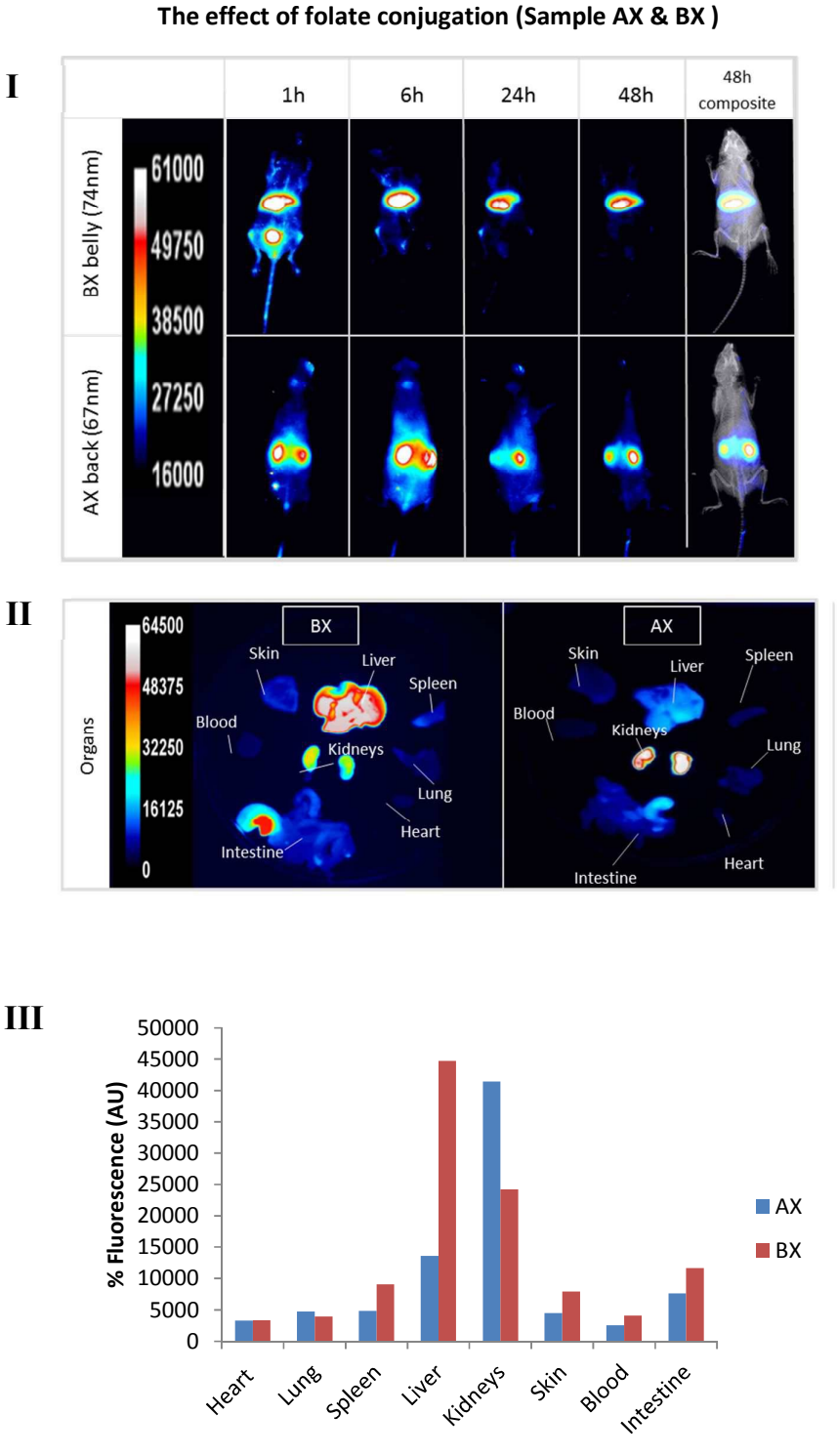

Figure 3. Experiment 3: The effect of folate conjugation. (I) comparison of *in vivo* fluorescence images two folate samples, BX and AX across different time courses after injection. (II) Organ fluorescence reflectance image at 48 hr. (III) Intensity comparison of sample BX and control sample AX in the organs after 48hr.

The effect of folate conjugation (Exp. 2, Figure 3)

The effect of folate conjugation was examined by comparing folate-labelled sample BX and the non-labelled sample AX, both of which are of similar size. As seen in the previous experiment, both polymers showed uptake in the kidneys, due to being crosslinked (Figure 3 II) In addition, both materials showed uptake in the liver, though this was dramatically higher in the folate labelled polymer BX. (Figure 3II) The results obtained here are consistent with previous work reported by us [39] and others [28, 40], where *in vivo* biodistribution of folate decorated drug and/or free folic acid exhibits high hepatic uptake. This may indicate that the particles were interacting with the folate receptor (FR) which is expressed in the liver (Kuppfer cells).[28] Zeta potential values of the samples were also measured and were found to be approximately around -10 mV. The slight negative charge of the particle may also contribute to the clearance of the particles through the RES pathway. [41] To further examine the difference in clearance mechanism, kidney accumulation is compared for sample AX and BX.

Folate labelled sample BX showed very high of fluorescence in the liver, *ex vivo* (Figure 3II). There is also a small, but measureable increase in the fluorescence uptake in the spleen, compared to the control polymer. This suggests that a small percentage of the particle is phagocytized by macrophages and cleared via RES pathway. However, the very high ratio of accumulation in the liver compared to the spleen suggests that the uptake is predominantly due to the expression of folate receptors in the liver and kidney. [39] This is supported by the similar-sized, non-labelled control polymer sample (AX), which shows much lower levels of fluorescence in the liver and spleen and significant fluorescence only in the kidneys at 48 hrs. Thus, the higher expression of folic acid leads to the higher levels of uptake in the liver, most likely through a receptor-ligand interaction.

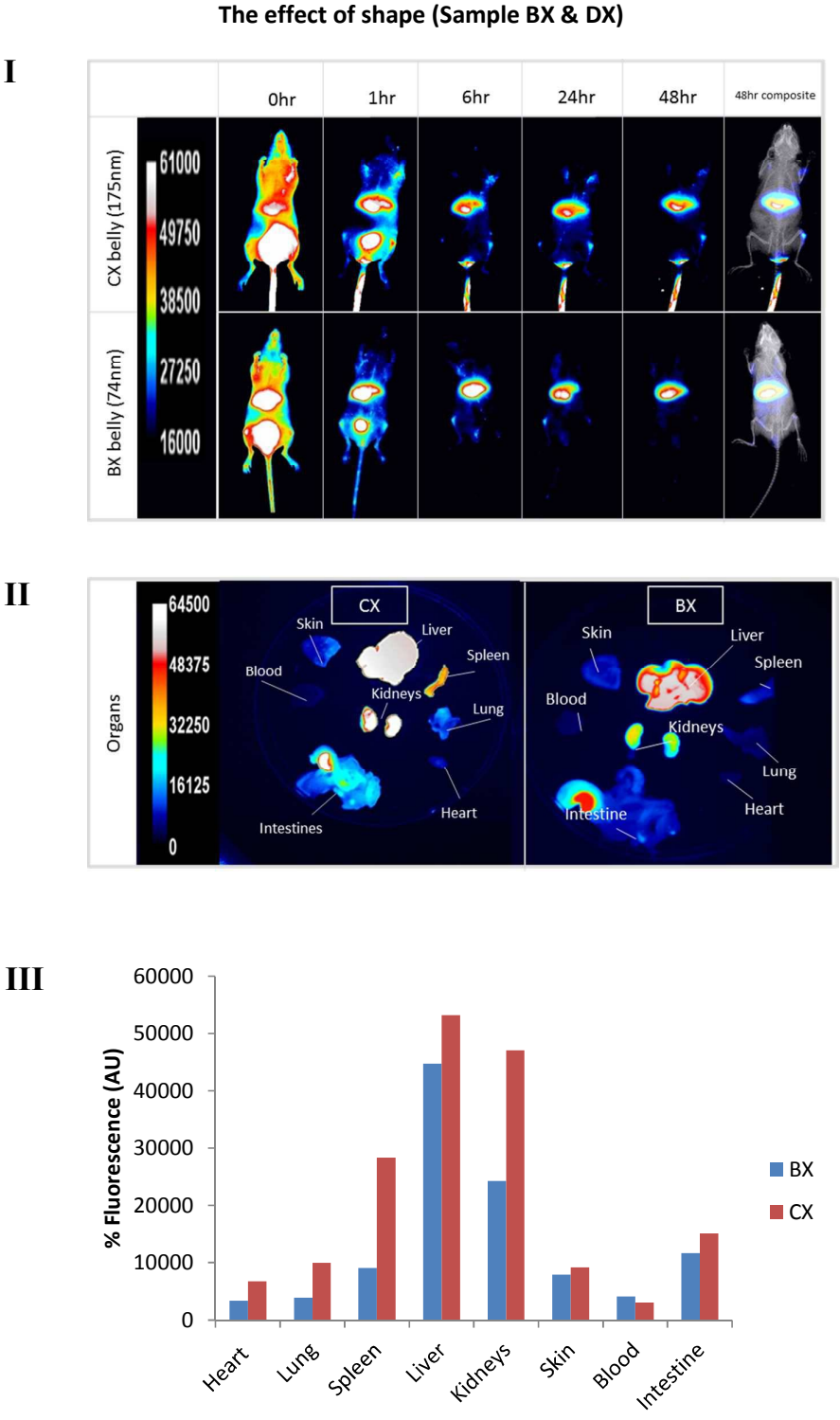

Figure 4. Experiment 4: The effect of shape. (I) comparison of in vivo fluorescence images two folate samples, DX and BX across different time courses after injection. (II) Organ fluorescence reflectance image at 48 hr. (III) Intensity comparison of sample CX and BX in the organs after 48hr.

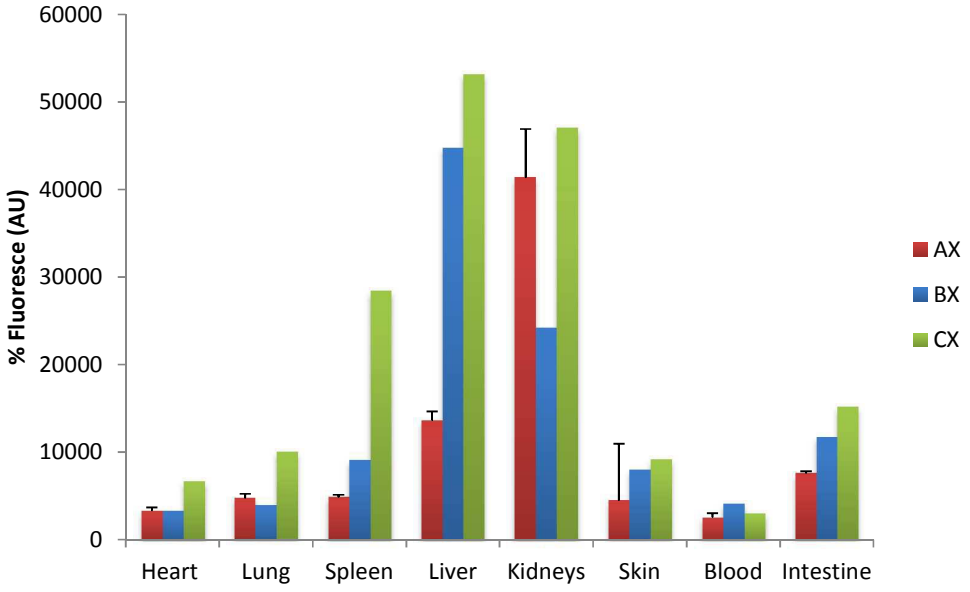

Figure 5. Normalised fluorescence intensity across all organs (% Fluorescence) for each sample.

Effect of shape (Exp 3, Figure 4)

Comparison of crosslinked folate samples BX (spherical) and DX (non-spherical) demonstrates the significant influence of the shape of the particle on its biodistribution (Scheme 2). It is observed that sample CX displayed the highest fluorescence intensity across all organs after 48 hours compared to all other samples discussed previously. The unusually high particle accumulation in organs may be the result of the irregular shape in sample CX. TEM images of this sample before and after crosslinking (Figure 1) showed a worm-like structure, while other samples showed a more spherical shape. Studies undertaken by Geng *et al.* compared the effects of filamentous particles on biodistribution compared to spherical shaped particles in both *in vivo* and *in vitro* environments. Their conclusions were in line with the results obtained in this study, where the worm-like micelles tended to be retained longer in the animal (Figure 5A, B). In addition, these filomicelles are able to mimic the behaviour of filamentous viruses within the body, thus allowing a higher probability for particles to enter diseased tissue.

While high fluorescence for both samples CX and BX was observed in organs such as liver, spleen, kidneys and the intestine that are responsible for clearance and excretion (Figure 5),

the ratio between the spleen and the liver is much higher in the worm like micelles, compared to the spherical particles. This is likely a direct consequence of activation of the RES clearance mechanism for the non-spherical particles. Besides the shape, the size of the particle might also influence accumulation within the organs. Ernsting *et al.* suggested that particle size of 50-100 nm is preferable in order to avoid clearance by liver macrophages [41], which supports our observation of a higher spleen to liver ratio in animals treated with CX (175nm) in contrast to BX (60 nm).

It is also worth noting that the signal within the spleen of the animal treated with sample CX was three times higher than that observed for sample BX and seven times higher than the control sample AX (See Figure 5). In addition, there was significant accumulation of sample CX in the organs that are not associated with RES, such as the heart and lungs which was higher than all other nanoparticles (A, AX and BX). This higher accumulation in organs such as the lung might be associated with the morphological characteristics as has been demonstrated by filamentous viruses when infecting human organs, such as Ebola filovirus and influenza filaments which are known to travel to the lung via bloodstream [42].

Conclusions

This study has confirmed the advantages of crosslinking micellar structures prior to utilization in living subjects. Most importantly, crosslinking enhances the structural integrity of the material, thus preventing dissociation during circulation in the body. Thus, crosslinked samples circulate longer in the body, as confirmed by increased fluorescence intensities in the organs at different times up to 48 hours as well as through *ex vivo* analyses. Folate conjugation further extends the circulation of crosslinked particles in the body when the particle formed worm-like shapes. However, these folate containing micelles are retained longer in most organs particularly in liver and kidney, while the naked particles exhibit faster clearance through bladder and intestine. This suggests that folic acid may not be the appropriate targeting ligand for drug delivery in this case, where folate-mediated accumulation in non-diseased tissue could lead to off-target toxicity.

The fate of the nanoparticles in the body is influenced by their morphologies. Slower rate of clearance was observed with worm-like shaped micelles compared to the spherical counterparts, thus filamentous particles showed much higher accumulation in various organs.

Although filomicelles could mimic the behavior of filamentous viruses which specifically prolong circulation and avoid rapid clearance mechanisms, the combination of the filamentous morphology along with folate targeting ligand on drug delivery systems might have adverse effects, where liver toxicity is likely to be increased in the body.

Acknowledgements

The authors would like to thank the Australian Research Council (ARC) for funding.

Supporting Information Available. Tables with absolute amounts for each of the block copolymerization including conversion, molecular weight data and ^{1}H-NMR characterization of the polymers; TEM micrographs and DLS data of all the self-assembled structures.

This material is available free of charge via the Internet at http://pubs.acs.org

References

1. Eliasof, S.; Lazarus, D.; Peters, C. G.; Case, R. I.; Cole, R. O.; Hwang, J.; Schluep, T.; Chao, J.; Lin, J.; Yen, Y.; Han, H.; Wiley, D. T.; Zuckerman, J. E.; Davis, M. E. *Proc. Nat. Academy Sci.* **2013,** 110, (37), 15127-15132.
2. Fang, J.; Nakamura, H.; Maeda, H. *Advanced Drug Delivery Reviews* **2011,** 63, (3), 136-151.
3. Fang, J.; Sawa, T.; Maeda, H., Factors and mechanism of "EPR" effect and the enhanced antitumor effects of macromolecular drugs including SMANCS. In *Advances in Experimental Medicine and Biology*, 2003; Vol. 519, pp 29-49.
4. Li, S.-D.; Huang, L. *Molecular Pharmaceutics* **2008,** 5, (4), 496-504.
5. Stolnik, S.; Illum, L.; Davis, S. S. *Adv. Drug Delivery Rev.* **1995,** 16, (2-3), 195-214.
6. Fang, J.; Nakamura, H.; Maeda, H. *Adv. Drug Delivery Rev.* **2011,** 63, (3), 136-151.
7. Maeda, H. *P. Jpn. Acad. B-PHYS* **2012,** 88, (3), 53-71.
8. Kim, Y.; Pourgholami, M. H.; Morris, D. L.; Stenzel, M. H. *Biomacromolecules* **2012,** 13, (3), 814-825.
9. Kim, Y.; Liemmawa, E. D.; Pourgholami, M. H.; Morris, D. L.; Stenzel, M. H. *Macromolecules* **2012,** 45, (13), 5451-5462.
10. Talelli, M.; Iman, M.; Varkouhi, A. K.; Rijcken, C. J.; Schiffelers, R. M.; Etrych, T.; Ulbrich, K.; van Nostrum, C. F.; Lammers, T.; Storm, G.; Hennink, W. E. *Biomaterials* **2010,** 31, (30), 7797-804.
11. Barkey, N. M.; Preihs, C.; Cornnell, H. H.; Martinez, G.; Carie, A.; Vagner, J.; Xu, L.; Lloyd, M. C.; Lynch, V. M.; Hruby, V. J.; Sessler, J. L.; Sill, K. N.; Gillies, R. J.; Morse, D. L. *Journal of Medicinal Chemistry* **2013,** 56, (16), 6330-6338.
12. Rijcken, C. J.; Snel, C. J.; Schiffelers, R. M.; van Nostrum, C. F.; Hennink, W. E. *Biomaterials* **2007,** 28, (36), 5581-5593.
13. Li, Y.; Xiao, K.; Luo, J.; Xiao, W.; Lee, J. S.; Gonik, A. M.; Kato, J.; Dong, T. A.; Lam, K. S. *Biomaterials* **2011,** 32, (27), 6633-6645.
14. Sun, G.; Hagooly, A.; Xu, J.; Nystrom, A. M.; Li, Z.; Rossin, R.; Moore, D. A.; Wooley, K. L.; Welch, M. J. *Biomacromolecules* **2008,** 9, (7), 1997-2006.
15. Gao, H.; Xiong, J.; Cheng, T.; Liu, J.; Chu, L.; Liu, J.; Ma, R.; Shi, L. *Biomacromolecules* **2013,** 14, (2), 460-467.
16. Hayama, A.; Yamamoto, T.; Yokoyama, M.; Kawano, K.; Hattori, Y.; Maitani, Y. *J. Nanosci. Nanotech.* **2007,** 8, 1-6.
17. Leamon, C. P.; Cooper, S. R.; Hardee, G. E. *Bioconjugate Chem.* **2003,** 14, (4), 738-747.
18. Leamon, C. P.; Low, P. S. *Drug Discov. Today* **2001,** 6, (1), 44-51.
19. Garcia-Bennett, A.; Nees, M.; Fadeel, B. *Biochem. Pharmacol.* **2011,** 81, (8), 976-984.
20. Xue, Y.; Tang, X.; Huang, J.; Zhang, X.; Yu, J.; Zhang, Y.; Gui, S. *Coll. Surf. B-Biointerfaces* **2011,** 85, (2), 280-288.
21. Yoo, H. S.; Park, T. G. *J. Control. Release* **2004,** 96, (2), 273-283.
22. Steichen, S. D.; Caldorera-Moore, M.; Peppas, N. A. *European Journal of Pharmaceutical Sciences* **2013,** 48, (3), 416-427.
23. Tu, Q.; Zhang, Y.; Liu, R.; Wang, J. C.; Li, L.; Nie, N.; Liu, A.; Wang, L.; Liu, W.; Ren, L.; Wang, X.; Wang, J. *Current Medicinal Chemistry* **2012,** 19, (19), 3152-3162.
24. Kim, D.; Gao, Z. G.; Lee, E. S.; Bae, Y. H. *Molecular Pharmaceutics* **2009,** 6, (5), 1353-1362.
25. Oyewumi, M. O.; Yokel, R. A.; Jay, M.; Coakley, T.; Mumper, R. J. *Journal of Controlled Release* **2004,** 95, (3), 613-626.

26. Gabizon, A.; Shmeeda, H.; Horowitz, A. T.; Zalipsky, S. *Advanced Drug Delivery Reviews* **2004,** 56, (8), 1177-1192.
27. Leamon, C. P.; Cooper, S. R.; Hardee, G. E. *Bioconjug Chem* **2003,** 14, (4), 738-747.
28. Rossin, R.; Pan, D.; Qi, K.; Turner, J. L.; Sun, X.; Wooley, K. L.; Welch, M. J. *J Nucl Med* **2005,** 46, (7), 1210-8.
29. Pino, P. d.; Pelaz, B.; Zhang, Q.; Maffre, P.; Nienhaus, G. U.; Parak, W. J. *Materials Horizons* **2014,** 1, (3), 301-313.
30. Yoo, H. S.; Park, T. G. *Journal of Controlled Release* **2004,** 96, (2), 273-283.
31. Kelland, L. *Nat Rev Cancer* **2007,** 7, (8), 573-84.
32. Boulikas, T.; Vougiouka, M. *Oncol Rep* **2004,** 11, (3), 559-95.
33. O'Dwyer, P. J.; Stevenson, J. P.; Johnson, S. W., Clinical Status of Cisplatin, Carboplatin, and Other Platinum-Based Antitumor Drugs. In *Cisplatin*, Verlag Helvetica Chimica Acta: 2006; pp 29-69.
34. Galanski, M.; Jakupec, M. A.; Keppler, B. K. *Curr Med Chem* **2005,** 12, (18), 2075-94.
35. Boase, N. R. B.; Blakey, I.; Thurecht, K. J. *Polymer Chemistry* **2012,** 3, (6), 1384-1389.
36. Stenzel, M. H.; Davis, T. P.; Fane, A. G. *Journal of Materials Chemistry* **2003,** 13, (9), 2090-2097.
37. Duong, H. T. T.; Huynh, V. T.; de Souza, P.; Stenzel, M. H. *Biomacromolecules* **2010,** 11, (9), 2290-2299.
38. Scarano, W.; Duong, H. T.; Lu, H.; De Souza, P. L.; Stenzel, M. H. *Biomacromolecules* **2013,** 14, (4), 962-75.
39. Rolfe, B. E.; Blakey, I.; Squires, O.; Peng, H.; Boase, N. R. B.; Alexander, C.; Parsons, P. G.; Boyle, G. M.; Whittaker, A. K.; Thurecht, K. J. *Journal of the American Chemical Society* **2014,** 136, (6), 2413-2419.
40. Shukla, S.; Wu, G.; Chatterjee, M.; Yang, W.; Sekido, M.; Diop, L. A.; Muller, R.; Sudimack, J. J.; Lee, R. J.; Barth, R. F.; Tjarks, W. *Bioconjug Chem* **2003,** 14, (1), 158-67.
41. Ernsting, M. J.; Murakami, M.; Roy, A.; Li, S.-D. *Journal of Controlled Release* **2013,** 172, (3), 782-794.
42. Yan, G.; Paul, D.; Shenshen, C.; Richard, T.; Manorama, T.; Tamara, M.; Dennis, E. D. *Nature Nanotechnology* **2007,** 2, (4), 249-255.

In vivo evaluation of folate decorated crosslinked micelles for the delivery of platinum anticancer drugs

Jeaniffer Eliezar, Wei Scarano, Nathan R. B. Boase, Kristofer J. Thurecht, Martina Stenzel